Experimental Evidence for the Spiral Spin Liquid in $LiYbO_2$

J. N. Graham,[1,2] N. Qureshi,[2] C. Ritter,[2] P. Manuel,[3] A. R. Wildes,[2] and L. Clark[1,*]
[1]School of Chemistry, University of Birmingham, Edgbaston, Birmingham B15 2TT, United Kingdom
[2]Institut Laue-Langevin, 71 avenue des Martyrs, CS20156, 38042 Grenoble Cédex 9, France
[3]ISIS Neutron and Muon Source, Rutherford Appleton Laboratory, Harwell Campus, Didcot OX11 0QX, United Kingdom

(Received 19 January 2023; accepted 20 March 2023; published 21 April 2023)

Spiral spin liquids are an exotic class of correlated paramagnets with an enigmatic magnetic ground state composed of a degenerate manifold of fluctuating spin spirals. Experimental realizations of the spiral spin liquid are scarce, mainly due to the prominence of structural distortions in candidate materials that can trigger order-by-disorder transitions to more conventionally ordered magnetic ground states. Expanding the pool of candidate materials that may host a spiral spin liquid is therefore crucial to realizing this novel magnetic ground state and understanding its robustness against perturbations that arise in real materials. Here, we show that the material $LiYbO_2$ is the first experimental realization of a spiral spin liquid predicted to emerge from the J_1-J_2 Heisenberg model on an elongated diamond lattice. Through a complementary combination of high-resolution and diffuse neutron magnetic scattering studies on a polycrystalline sample, we demonstrate that $LiYbO_2$ fulfills the requirements for the experimental realization of the spiral spin liquid and reconstruct single-crystal diffuse neutron magnetic scattering maps that reveal continuous spiral spin contours—a characteristic experimental hallmark of this exotic magnetic phase.

DOI: 10.1103/PhysRevLett.130.166703

Magnetic states with unusual spin textures, such as magnetic skyrmions or vortices, are important both from a fundamental perspective as well as for their potential applications in emerging technologies [1–4]. A lesser-explored manifestation of such unusual spin textures is the spiral spin liquid, a correlated paramagnetic state composed of a macroscopically degenerate manifold of fluctuating spin spirals that form closed contours or surfaces in reciprocal space [5–8]. From a theoretical perspective, spiral spin liquids have been predicted to exist in both two and three dimensions within the context of the frustrated J_1-J_2 Heisenberg model, for example, in honeycomb or diamond lattices [5,9,10]. Experimentally, the search for the spiral spin liquid has focused on its realization within cubic spinels, AB_2X_4, in which the A site forms a three-dimensional diamond lattice [11–21].

The diamond lattice can be considered as two interpenetrating fcc sublattices, with nearest-neighbor (NN) J_1 and next-nearest-neighbor (NNN) J_2 exchange interactions acting between and within sublattices, respectively (see Supplemental Material [22], Fig. S1) [7,8,23]. When the J_1 exchange interaction dominates, the diamond lattice is geometrically unfrustrated, leading to the formation of conventional ferromagnetic or Néel ordered magnetic ground states. However, the bipartite nature of the diamond lattice means that the exchanges can be readily tuned, and when $J_2/|J_1| \geq 1/8$, the system is expected to form a spiral spin liquid ground state [7,8,23]. Several cubic spinels have been identified as candidates for this model, including $MnSc_2S_4$ [11,12], $NiRh_2O_4$ [13–15], and $CoAl_2O_4$ [16,17]. In particular, $MnSc_2S_4$ is considered the first experimental realization of the spiral spin liquid on a perfect diamond lattice, with the observation of the characteristic spiral spin surface in single-crystal diffuse neutron magnetic diffraction measurements [11]. However, experimentally, a true, continually fluctuating spiral spin liquid is still a rare occurrence. More often, the degeneracy of the system is lifted via an order-by-disorder mechanism, collapsing the fluctuating state into one with a single, long-range ordered spin helix [7,8,23].

It was widely accepted that structural distortions to the perfect diamond lattice trigger this order-by-disorder mechanism, and therefore, are detrimental to the realization of the spiral spin liquid phase. However, a recent re-imagining of this theory determined that a spiral spin liquid could still be realized under a tetragonal distortion to the diamond lattice [7,23,24]. The key to this elongated diamond lattice model is to consider the effect of the tetragonal distortion on the superexchange pathways. In the perfect diamond lattice, J_2 describes the next-nearest neighbor superexchange pathway, but in the elongated

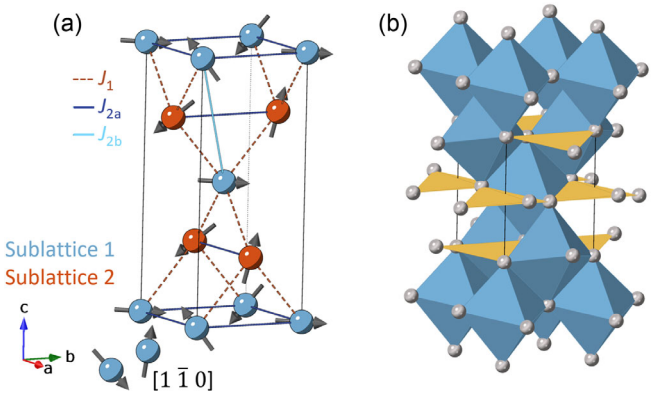

FIG. 1. (a) The elongated diamond lattice—such as that formed from Yb^{3+} moments in $LiYbO_2$—can be considered as two equivalent sublattices shown by the blue and orange spheres with NN J_1 (dashed orange) and NNN J_2 (solid blue) exchanges acting between and within sublattices, respectively. In the undistorted diamond lattice, $J_{2a} = J_{2b}$, but in the elongated diamond lattice model, $|J_1| \approx J_{2a} \gg J_{2b}$, which introduces magnetic frustration. Moment orientations are shown by the gray arrows for the incommensurate helical structure with $\mathbf{k} = (0.3915(2), \pm 0.3915(2), 0)$ determined from WISH data analysis. Moments are shown propagating along the $[1\ \bar{1}\ 0]$ direction. (b) $LiYbO_2$ adopts the tetragonal $I4_1/amd$ structure where Yb^{3+} ions (light blue polyhedra) form an elongated diamond network with tetrahedrally coordinated Li^+ ions (yellow polyhedra) lying in between.

model, J_2 is spilt into two nonequivalent exchanges, J_{2a} and J_{2b} [Fig. 1(a)]. Now, the superexchange pathways J_1 and J_{2a} ($J_2 \| \langle 100 \rangle$ in the undistorted lattice) may be nearly equivalent in length and substantially shorter than the J_{2b} pathway ($J_2 \| \langle 111 \rangle$ in the undistorted lattice). In this case, the strength of the J_{2b} exchange interaction is assumed negligible in comparison to J_1 and J_{2a}. If the magnitudes of J_1 and J_{2a} are comparable, this elongated diamond lattice is expected to be frustrated and may lead to the emergence of a novel spiral spin liquid ground state.

One potential candidate for the realization of this J_1-J_2 Heisenberg model on an elongated diamond lattice is $NaCeO_2$. This system adopts a tetragonal $I4_1/amd$ structure with an axial elongation of $c/\sqrt{2}a = 1.63$, which was considered sufficient to render J_{2b} negligible [25]. However, neutron diffraction data for $NaCeO_2$ show that it forms a commensurate Néel ordered ground state below 3.18 K due to $J_1 \gg J_{2a}$. This is not surprising, given theory predicts that when $J_{2a} > 0$ (antiferromagnetic), the spiral spin liquid phase exists within a relatively narrow region between commensurate ferromagnetic ($-4 < J_1/J_{2a}$) and antiferromagnetic ($J_1/J_{2a} < 4$) phases [23,24]. Thus, here we turn our attention to $LiYbO_2$, which like $NaCeO_2$ adopts a tetragonal $I4_1/amd$ structure [Fig. 1(b)], but importantly, the ratio of exchange parameters has been determined as $J_1 = 1.426 J_{2a} > 0$, placing $LiYbO_2$ within the boundary of the spiral spin liquid phase of an elongated diamond lattice [24,26].

However, a recent investigation of $LiYbO_2$ concluded that it is not an experimental realization of the spiral spin liquid [24,27]. Theory allows for an incommensurate helical structure propagating along the diagonal of the tetragonal basal plane [$\mathbf{k} = (\delta, \pm\delta, 0)$], which acts across the two Yb^{3+} sublattices. Critically, however, the moments on these sublattices must have a fixed phase difference of $\phi = \pi$ to allow moments to rotate along all bonds between the sublattices equivalently [24]. Experimentally, ϕ was found to be only 0.58π for $LiYbO_2$, resulting in a staggering effect between moments, and additional perturbations to the J_1-J_2 Heisenberg model on the elongated diamond lattice were required to explain these previous experimental results. The possibility for disorder, for example, in the local Yb^{3+} environment, was proposed as the cause for this discrepancy in the phase angle, but structural disorder was not resolvable within the diffraction measurements presented [24]. Furthermore, the ordered moment size determined from previous powder neutron diffraction measurements was only 84% of the expected full ordered moment of the $S_{\text{eff}} = \frac{1}{2}$ Yb^{3+} ions in $LiYbO_2$, indicating that the true nature of its ground state remained elusive. Thus, here we combine complementary high-resolution and diffuse neutron magnetic scattering measurements on $LiYbO_2$ to recover the full Yb^{3+} moment and reexamine the phase angle, ϕ. In doing so, we identify $LiYbO_2$ as the first experimental realization of the J_1-J_2 Heisenberg spiral spin liquid on the elongated diamond lattice.

A high-quality polycrystalline sample of $LiYbO_2$ was prepared via a solid-state synthesis method described in the Supplemental Material [22]. Time-of-flight neutron powder diffraction data were collected on the long-wavelength WISH diffractometer at the ISIS Neutron and Muon Source [28,29]. Magnetic Bragg peaks measured between 0.08 and 1.2 K were isolated by subtracting a paramagnetic dataset collected at 5 K. Below 450 mK there are several magnetic Bragg peaks in the temperature-subtracted diffraction data that may be indexed by an incommensurate helical magnetic model. Figure 2(a) shows the Rietveld refinement of this model against the data measured at 80 mK, where the propagation vector was refined to the doubly degenerate $\mathbf{k} = (0.3915(2), \pm 0.3915(2), 0)$ with a schematic of the corresponding magnetic structure shown in Fig. 1(a) [30,31]. The refined moment, $\mu_{\text{order}} = 0.63(1)\ \mu_B$ is only ~40% of the expected full ordered moment size, $\mu_{\text{exp}} = gS\mu_B = 1.5\ \mu_B$, assuming $S_{\text{eff}} = 1/2$ and $g = 3$ [24]. The phase angle between the two sublattices of Yb^{3+} moments refined to $\phi = 1.15(5)\pi$. Refinements as a function of temperature have no variation below 450 mK in $\mathbf{k}$, μ_{order} or ϕ [Figs. 2(c)–2(e), respectively].

Previous characterization of $LiYbO_2$ discounted its candidacy as a spiral spin liquid based on the measured phase angle between the sublattices, $\phi = 0.58\pi$, being in disagreement with the theoretical prediction of $\phi = \pi$ [24].

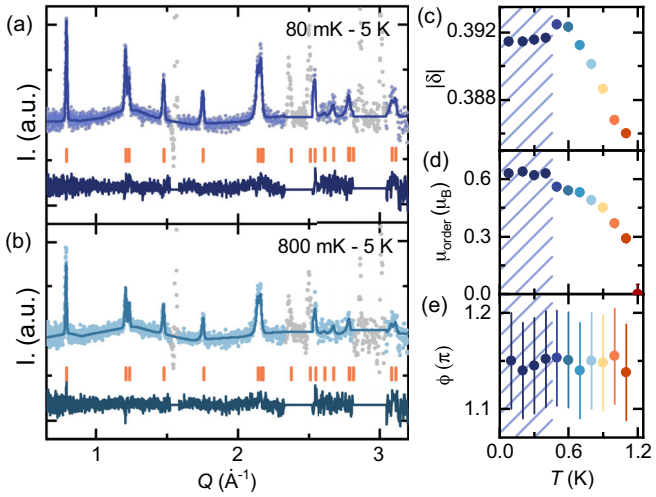

FIG. 2. Refinement of the incommensurate helical magnetic structure within the spiral spin liquid phase of $LiYbO_2$ at (a) 80 mK ($R_{mag} = 13.1\%$, $\chi^2 = 3.06$) and (b) 800 mK ($R_{mag} = 7.49\%$, $\chi^2 = 2.96$) from data collected on WISH. In both (a) and (b) data points and fits are shown in blue, difference curves in dark blue, magnetic Bragg reflections by the orange tickmarks, and excluded data from the paramagnetic subtraction in gray. Evolution of refined parameters (c) propagation vector, $\mathbf{k} = (\delta, \pm\delta, 0)$, (d) ordered moment size, μ_{order} and (e) phase angle, ϕ. A transition occurs at 450 mK, where $\mathbf{k}$ and μ_{order} change from evolving as a function of temperature to being constant in temperature. This locking-in of the parameters coincides with a peak in previous heat capacity measurements of $LiYbO_2$ [24].

However, the refinement of the phase angle in this work, $\phi = 1.15(5)\pi$ is consistent with the theoretical prediction and, therefore, verifies that $LiYbO_2$ maps onto the J_1-J_2 Heisenberg model on an elongated diamond lattice. In the previous experimental study, this misassignment of ϕ likely stemmed from the need to pelletize the polycrystalline sample for the in-field neutron diffraction measurements presented. This, in turn, required the inclusion of a significant preferred orientation correction during the Rietveld analysis of the powder neutron diffraction data [24]. All measurements presented here were performed on a loose powder, therefore, preferred orientation is not an issue, as confirmed through Rietveld refinement of the chemical structure against high-resolution powder neutron difffraction data collected on the D2B instrument at the Institut Laue-Langevin (ILL) using `Mag2Pol` (Supplemental Material [22], Fig. S2) [31–33]. Additionally, the magnetic structure is best described by a propagation vector of $\mathbf{k} = (\delta, \pm\delta, 0)$, which is the correct form required to generate the spiral spin liquid phase [23,24,34]. The ratio of exchange parameters determined from this helical structure, $J_1 = 1.343(4)J_{2a} > 0$ places $LiYbO_2$ directly within the spiral spin liquid phase. Therefore, we propose that $LiYbO_2$ is the first material to fulfill experimentally all of the conditions required for the observation of the spiral spin liquid in the J_1-J_2 Heisenberg model on an elongated diamond lattice [24].

In addition to this spiral spin liquid ground state, time-of-flight neutron powder diffraction data reveal that an intermediary phase exists between 450 mK and 1.2 K. This phase is similar to the one determined below 450 mK but evolves with temperature. An example of the Rietveld analysis of this intermediary phase is shown in Fig. 2(b) for a dataset measured on WISH at 800 mK. Refinement as a function of temperature reveals three key conclusions about the intermediary phase: (i) the propagation vector, $\mathbf{k}$, varies with temperature but always takes the form $\mathbf{k} = (\delta, \pm\delta, 0)$, (ii) the ordered moment size, μ_{order}, gradually reduces from $0.63(1)\ \mu_B$ to zero by 1.2 K, but (iii) the phase angle between the sublattices, $\phi = 1.15(5)\pi$ remains constant throughout the phase, as shown in Figs. 2(c)–2(e), respectively. Therefore, this intermediary phase still fulfills the requirements of the spiral spin liquid [24].

While from an average-structure perspective the spiral spin liquid phase in $LiYbO_2$ has now been confirmed, a remaining question is to understand why the experimentally determined moment size is significantly reduced in comparison to the full ordered moment. The defining experimental signature of the spiral spin liquid is a broad continuous ring of neutron magnetic scattering in reciprocal space [11], caused by the correlated fluctuations of spin spirals. Thus, it seems plausible that the remaining missing moment must be contained within these spin spiral fluctuations, which will give the characteristic diffuse magnetic scattering of the spiral spin liquid. To confirm this hypothesis, diffuse polarized neutron scattering measurements were performed on D7 at the ILL [33,35,36] as described in the Supplemental Material [22]. The time-equal magnetic cross sections of $LiYbO_2$ measured on D7 are presented in Fig. 3(a). Paramagnetic behavior is observed in the magnetic scattering at 25 K and was modeled using a $\langle j_0 \rangle$ analytical approximation of the Yb^{3+} form factor [37]. The approximation assumes a $S_{eff} = 1/2$ ground state for Yb^{3+} with $g = 3$, which is valid given the integration window of D7 ($-20 \leq \Delta E < 3$ meV) is well below the previously observed crystal field excitations for $LiYbO_2$ [24]. Beneath the magnetic Bragg peaks at 50 and 800 mK there is significant structure in the diffuse magnetic scattering, which is also visible in the WISH data (Fig. 2). Most prominent is the broad feature centered around $Q = 1.2$ Å^{-1}, which has virtually no change in size or shape in the diffuse scattering between 50 mK and 1.5 K.

The 50 and 800 mK data were modeled using a modified version of the `SPINVERT` program (`SPINVERT + Bragg`) in order to simultaneously fit the magnetic Bragg and diffuse features (Supplemental Material [22,38,39]) [40,41]. A challenging aspect of this analysis was the incommensurate nature of the magnetic structure, as `SPINVERT` relies on periodic boundary conditions to generate a supercell. Therefore, the propagation vector

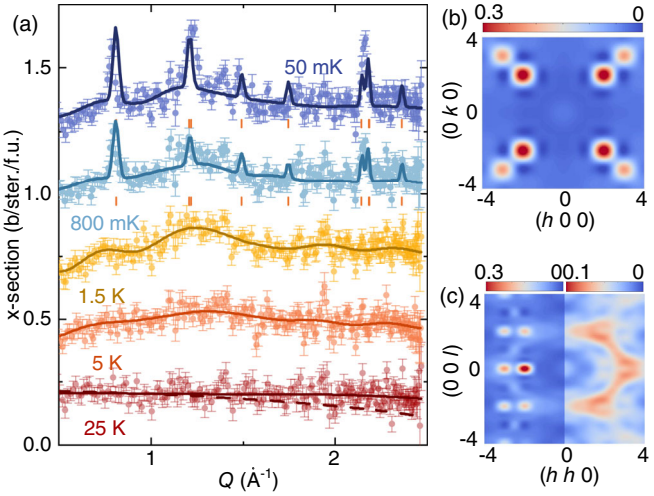

FIG. 3. (a) Neutron magnetic scattering cross section for $LiYbO_2$ as measured on D7. At 50 and 800 mK, both magnetic Bragg and correlated diffuse scattering are observed for the spiral spin liquid phase, which were analyzed simultaneously with SPINVERT + Bragg by making the commensurate approximation to $\mathbf{k} = (0.4, \pm 0.4, 0)$ (orange tickmarks). Data at 1.5 and 5 K were fit with SPINVERT (solid lines) and 25 K by a paramagnetic form factor of Yb^{3+} ions (dashed line). Data have been vertically shifted by 0.3 b./ster./f.u. for clarity. Single-crystal reconstructions from powder data analysis at 50 mK, (b) positions of incommensurate magnetic Bragg peaks in the $(h\,k\,0)$ plane and (c) the signature of the spiral spin liquid, a continuous diffuse ring in the $(h\,h\,l)$ plane (left: total magnetic scattering, right: magnetic diffuse scattering only, magnetic Bragg peaks have been excluded to show the diffuse ring more clearly). Intensities have been normalized to absolute units according to the color bars.

determined on WISH was approximated to the commensurate $\mathbf{k} = (0.4, \pm 0.4, 0)$, and a supercell of $10 \times 10 \times 4$ unit cells was constructed. Spins were allowed complete rotational freedom, as introducing anisotropy to refine in a conical fashion did not make any difference to the fit. The resultant fits are shown in Fig. 3(a) and emulate the main features of the data extremely well. Additionally, the diffuse-only data measured at 1.5 and 5 K were fit with SPINVERT using a supercell of $6 \times 6 \times 3$ unit cells. The data from D7 are normalized to an absolute intensity scale, and therefore, the scale factor from SPINVERT is directly related to the moment size. This was separated into the proportion of the moment which is ordered and disordered, and these values are summarized in Table I.

Thus, we show that the full moment of $LiYbO_2$ can be obtained through the simultaneous refinement of magnetic Bragg and diffuse scattering. It is important to note that the moments obtained from each instrument are not directly comparable due to the definitions used, Rietveld method: $\mu^2 = g^2 S^2 \mu_B^2$ and SPINVERT + Bragg analysis: $\mu^2 = g^2 S(S+1)\,\mu_B^2$. Assuming both have $S_{\text{eff}} = 1/2$ and $g = 3$, [24] a full moment size of $\mu = 1.5\ \mu_B$ for WISH and $\mu = 2.6\ \mu_B$ for D7 is expected. At base temperature, μ_{order} accounts for 40% and 30% of the expected moments for WISH and D7, respectively. The difference between the two methods is likely due to the incommensurate-commensurate approximation in the SPINVERT + Bragg analysis which underfits some of the magnetic Bragg peaks, most prominently, at $Q = 2.16$ Å^{-1}. This is a limitation of the reverse Monte Carlo analysis at this time, however, given the complexity of the magnetic structure, and the agreement with the WISH results, we conclude that the moment sizes presented here are an accurate description of the system.

TABLE I. Summary of experimental magnetic moments for $LiYbO_2$, with μ_{order} from Rietveld analysis of WISH data and μ_{total} split into helically ordered, μ_{order} and correlated short-range ordered, μ_{disorder} components from SPINVERT + Bragg analysis of D7 data. Base temperatures for the WISH and D7 experiments are 80 mK and 50 mK, respectively.

	WISH	D7		
T (K)	μ_{order} (μ_B)	μ_{order} (μ_B)	μ_{disorder} (μ_B)	μ_{total} (μ_B)
Base	0.63(1)	0.80(1)	1.80(1)	2.60(1)
0.8	0.49(1)	0.67(2)	1.92(2)	2.59(2)
1.5	⋯	⋯	2.73(2)	2.73(2)
5	⋯	⋯	2.74(2)	2.74(2)
25	⋯	⋯	2.76(2)	2.76(2)

Reconstructions of single-crystal neutron magnetic diffraction patterns were calculated from fits of the 50 mK D7 powder data using SCATTY [40,42]. Figure 3(b) shows the simulation for the $(h\,k\,0)$ plane, which reveals strong magnetic intensity at the expected magnetic Bragg peak positions. Because of the calculation method of the single-crystal scattering plane, the magnetic Bragg peaks appear artificially broadened in the simulation. The $(h\,h\,l)$ plane, being a slice diagonally through the $(h\,k\,0)$ plane, is shown in Fig. 3(c), where the ring of diffuse scattering, representing the contoured spiral surface, can clearly be seen. This is the expected manifestation of single-crystal diffuse magnetic neutron scattering for a spiral spin liquid [11] and, therefore, further corroborates that the analysis and conclusions presented here for the magnetic ground state of $LiYbO_2$ are correct.

The spin-spin correlation function, $\langle \mathbf{S}(0) \cdot \mathbf{S}(r) \rangle$, for $LiYbO_2$ was calculated by SPINCORREL [40,42] from fits to the D7 data. The correlations at 50 mK [Fig. 4(a)] are in good agreement with the predicted correlations for a helically ordered state (Supplemental Material [22]). The modified SPINVERT + Bragg analysis allows for the proportion of correlations to be broken down into short- and long-range ordered contributions, as shown by the open and closed markers, respectively, in Fig. 4(b). The temperature dependence of these correlations quantifies the observations made in the D7 data. Namely, correlations that contribute to the diffuse scattering are temperature

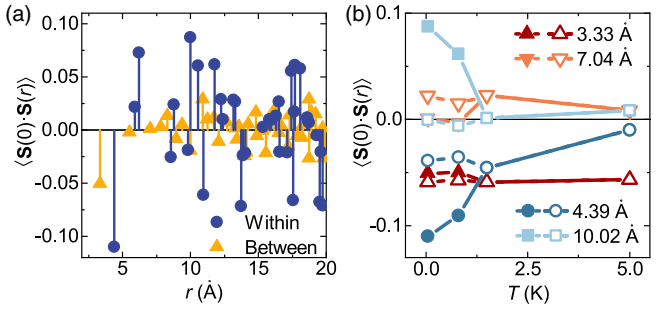

FIG. 4. (a) Spin-spin correlation function, $\langle \mathbf{S}(0) \cdot \mathbf{S}(r) \rangle$, as a function of interatomic distance r for $LiYbO_2$ at 50 mK. Correlations are divided into those within (blue) and between sublattices (yellow). (b) Spin-spin correlation function, $\langle \mathbf{S}(0) \cdot \mathbf{S}(r) \rangle$, as a function of temperature showing the relative contributions of the short-range (open, constant) and long-range (closed, decreasing) correlations.

independent between 50 mK and 1.5 K but ordered contributions are temperature dependent.

Taken together, this complementary neutron scattering study shows that a new family of materials—those with an elongated diamond lattice—provides an experimentally achievable route to the spiral spin liquid. There are three conditions needed to confirm the spiral spin liquid phase: (i) a phase angle ϕ between the magnetic sublattices that is equal to π, (ii) a propagation vector of the form $\mathbf{k} = (q, q, 0)$, and (iii) a ratio of exchange interactions of $-4 < J_1/|J_2| < 4$. Through the results presented here, we have confirmed conditions (i) $\phi = 1.15(5)\pi$, (ii) $\mathbf{k} = (\delta, \pm\delta, 0)$, and (iii) $J_1 = 1.343(4)J_{2a} > 0$ below 450 mK. Further, conclusive evidence for the spiral spin liquid phase was revealed by the continuous spin spiral contours in the $(h\,h\,l)$ plane from single-crystal reconstructions of the diffuse powder scattering data. Future studies on single crystals would thus confirm the exchange parameters through inelastic neutron scattering and verify our magnetic diffuse scattering simulations. The expected full moment of $LiYbO_2$ was recovered through the analysis of diffuse neutron scattering measurements and is split between the long- and short-range contributions characteristic of the spiral spin liquid. To date, only $LiYbO_2$ [24,27] and $NaCeO_2$ [25] have been explored within the context of the J_1-J_2 Heisenberg model on the elongated diamond lattice, but their differing ratios of exchange parameters lead to the formation of distinct magnetic ground states. However, we have proven that for $LiYbO_2$, a spiral spin liquid ground state is achievable within this new geometry and, therefore, future studies may also probe the robustness of the model to understand the relative importance of the stretching ratio, magnitude of exchange interactions, and superexchange pathways when designing new candidate systems.

We are grateful to S. D. Wilson (UC Santa Barbara), M. M. Bordelon (Los Alamos National Laboratory), and J. A. M. Paddison (Oak Ridge National Laboratory) for helpful discussions and advice in completing this work. We acknowledge the University of Birmingham and the Institut Laue-Langevin for the Ph.D. Studentship of J. N. Graham and the UKRI Science and Technology Facilities Council for the provision of beam time.

*Corresponding author.
l.m.clark@bham.ac.uk

[1] M. Augustin, S. Jenkins, R. Evans, K. S. Novoselov, and S. E. J. G., Nat. Commun. **12**, 185 (2021).
[2] M. Hervé, B. Dupé, R. Lopes, M. Bottcher, M. D. Martins, T. Balashov, L. Gerhard, J. Sinova, and W. Wulfhekel, Nat. Commun. **9**, 1015 (2018).
[3] Y. Tokura and N. Kanazawa, Chem. Rev. **121**, 2857 (2021).
[4] B. Göbel, I. Mertig, and O. A. Tretiakov, Phys. Rep. **895**, 1 (2021).
[5] X.-P. Yao, J. Q. Liu, C.-J. Huang, X. Wang, and G. Chen, Front. Phys. **16**, 53303 (2021).
[6] N. Niggermann, M. Hering, and J. Reuther, J. Phys.: Condens. Matter. **32**, 024001 (2020).
[7] S. B. Lee and L. Balents, Phys. Rev. B **78**, 144417 (2008).
[8] F. L. Buessen, M. Hering, J. Reuther, and S. Trebst, Phys. Rev. Lett. **120**, 057201 (2018).
[9] S. Gao, M. A. McGuire, Y. Liu, D. L. Abernathy, C. Cruz, M. Frontzek, M. B. Stone, and A. D. Christianson, Phys. Rev. Lett. **128**, 227201 (2022).
[10] S. B. Lee, J.-S. Jeong, K. Hwang, and Y. B. Kim, Phys. Rev. B **90**, 134425 (2014).
[11] S. Gao, O. Zaharko, V. Tsurkan, Y. Su, J. S. White, G. S. Tucker, B. Roessli, F. Bourdarot, R. Sibille, D. Chernyshov, T. Fennell, A. Loidl, and C. Rüegg, Nat. Phys. **13**, 157 (2017).
[12] Y. Iqbal, T. Müller, H. O. Jeschke, R. Thomale, and J. Reuther, Phys. Rev. B **98**, 064427 (2018).
[13] J. R. Chamorro, L. Ge, J. Flynn, M. A. Subramanian, M. Mourigal, and T. M. McQueen, Phys. Rev. Mater. **2**, 034404 (2018).
[14] S. Das, D. Nafday, T. SahaDasgupta, and A. Paramekanti, Phys. Rev. B **100**, 140408(R) (2019).
[15] F. L. Buessen, M. Hering, J. Reuther, and S. Trebst, Phys. Rev. Lett. **120**, 057201 (2018).
[16] S. Ghara, N. V. Ter-Oganessian, and A. Sundaresan, Phys. Rev. B **95**, 094404 (2017).
[17] G. J. MacDougall, D. Gout, J. L. Zarestky, G. Ehlers, A. Podlesnyak, M. A. McGuire, D. Mandrus, and S. E. Nagler, Proc. Natl. Acad. Sci. U.S.A. **108**, 15693 (2011).
[18] R. S. Dissanayaka Mudiyanselage, H. Wang, O. Vilella, M. Mourigal, G. Kotliar, and W. Xie, J. Am. Chem. Soc. **144**, 11933 (2022).
[19] N. Tristan, J. Hemberger, A. Krimmel, H.-A. Krug von Nidda, V. Tsurkan, and A. Loidl, Phys. Rev. B **72**, 174404 (2005).
[20] L. Ge, J. Flynn, J. A. M. Paddison, M. B. Stone, S. Calder, M. A. Subramanian, A. P. Ramirez, and M. Mourigal, Phys. Rev. B **96**, 064413 (2017).
[21] X. Bai, J. A. M. Paddison, E. Kapit, S. M. Koohpayeh, J.-J. Wen, S. E. Dutton, A. T. Savici, A. I. Kolesnikov,

G. E. Granroth, C. L. Broholm, J. T. Chalker, and M. Mourigal, Phys. Rev. Lett. **122**, 097201 (2019).
[22] See Supplemental Material at http://link.aps.org/supplemental/10.1103/PhysRevLett.130.166703 for details on sample preparation, experimental set up and analysis of D7 data.
[23] D. Bergman, J. Alicea, E. Gull, S. Trebst, and L. Balents, Nat. Phys. **3**, 487 (2007).
[24] M. M. Bordelon, C. Liu, L. Posthuma, E. Kenney, M. J. Graf, N. P. Butch, A. Banerjee, S. Calder, L. Balents, and S. D. Wilson, Phys. Rev. B **103**, 014420 (2021).
[25] M. M. Bordelon, J. D. Bocarsly, L. Posthuma, A. Banerjee, Q. Zhang, and S. D. Wilson, Phys. Rev. B **103**, 024430 (2021).
[26] Y. Hashimoto, M. Wakeshima, K. Matsuhira, Y. Hinatsu, and Y. Ishii, Chem. Mater. **14**, 3245 (2002).
[27] E. M. Kenney, M. M. Bordelon, C. Wang, H. Luetkens, S. D. Wilson, and M. J. Graf, Phys. Rev. B **106**, 144401 (2022).
[28] L. C. Chapon, P. Manuel, P. G. Radaelli, C. Benson, L. Perrott, S. Ansell, N. J. Rhodes, D. Raspino, D. Duxbury, E. Spill, and J. Norris, Neutron News **22**, 22 (2011).
[29] J. N. Graham, P. Manuel, A. R. Wildes, and L. Clark, *ISIS Neutron and Muon Source*, 10.5286/ISIS.E.RB2200001-1 (Springer, New York, 2022), data for WISH experiment.
[30] J. Rodriguez-Carvajal, Physica (Amsterdam) **192B**, 55 (1993).
[31] N. Qureshi, J. Appl. Crystallogr. **52**, 175 (2019).
[32] A. W. Hewat, Mater. Sci. Forum **9**, 69 (1986).
[33] J. N. Graham, C. Ritter, L. Clark, and A. R. Wildes, *Institut Laue-Langevin*, 10.5291/ILL-DATA.5-32-921 (Springer, New York, 2021), data for D7 and D2B experiments.
[34] J.-S. Bernier, M. J. Lawler, and Y. B. Kim, Phys. Rev. Lett. **101**, 047201 (2008).
[35] J. R. Stewart, P. P. Deen, K. H. Andersen, H. Schober, J.-F. Barthélémy, J. M. Hillier, A. P. Murani, T. Hayes, and B. Lindenau, J. Appl. Crystallogr. **42**, 69 (2009).
[36] W. Schweika, J. Phys. Conf. Ser. **211**, 012026 (2010).
[37] P. J. Brown, *International Tables of Crystallography* (2006), Vol. C, pp. 454–461.
[38] J. Rossat-Mignod, in *Neutron Scattering*, Methods in Experimental Physics, edited by K. Skjold and D. L. Price (Academic Press Inc., New York, 1987), Vol. 23C.
[39] T. Fennell, L. Mangin-Thro, H. Mutka, G. Nilsen, and A. Wildes, Nucl. Instrum. Methods Phys. Res., Sect. A **857**, 24 (2017).
[40] J. A. M. Paddison and A. L. Goodwin, Phys. Rev. Lett. **108**, 017204 (2012).
[41] J. A. M. Paddison, H. S. Ong, J. O. Hamp, P. Mukherjee, X. Bai, M. G. Tucker, N. P. Butch, C. Castelnovo, M. Mourigal, and S. E. Dutton, Nat. Commun. **7**, 13842 (2016).
[42] J. A. M. Paddison, J. R. Stewart, and A. L. Goodwin, J. Condens. Matter Phys. **25**, 454220 (2013).